Coherent Detection and Channel Coding for Bistatic Scatter Radio Sensor Networking

Nikos Fasarakis-Hilliard, Panos N. Alevizos, *Student Member, IEEE*, and Aggelos Bletsas, *Senior Member, IEEE*

***Abstract*—With rapid advances of scatter radio systems, the principle of reflection rather than active transmission employed by backscatter sensor networks has emerged as a potential key enabler for low-cost, large-scale and dense ubiquitous sensor networks. Despite the presence of three different unknown channel links due to the bistatic setup (i.e., carrier emitter and receiver are dislocated), as well as multiple unknown scatter radio-related parameters, this work offers a novel *coherent* receiver of frequency-shift keying (FSK) modulation for the bistatic scatter radio channel. Furthermore, with the objective of range maximization, specific *short* block-length cyclic channel codes are utilized. The proposed approach requires minimum encoding complexity, ideal for resource-constrained, ultra-low power (e.g. microcontroller unit-based), low-bit rate scatter radio tags, adheres to simple low-complexity decoding at the receiver and achieves high-order signal diversity. Analysis is followed by experimental validation with a commodity software-defined radio (SDR) reader and a custom scatter radio tag; tag-to-reader ranges up to 150 meters are demonstrated with as little as 20 milliWatt transmission power, increasing sensing ranges by approximately 10 additional meters, compared to state-of-the-art bistatic scatter radio receivers. With the imminent emergence of backscatter sensor networks, this work serves as a small step forward towards the realization of low-cost, low-power, increased-range, wireless sensing applications.**

***Index Terms*—Bistatic backscatter sensor networks, coherent detection, cyclic channel codes, soft-decision decoding, increased bistatic ranges.**

I. Introduction

Dramatic advances in sensor technology are driving the ubiquitous deployment of large-scale wireless sensor networks (WSNs) to unprecedented levels. Current state-of-the-art WSNs have been seemingly integrated into many aspects of every-day life and are constantly deployed for a plethora of monitoring and/or control applications in some of the most diverse fields [1]. One of the most promising applications of WSNs is that of environmental monitoring, where literally hundreds or thousands of sensors are deployed to monitor various environmental variables at scales and resolutions previously considered impossible to achieve. The dream of ubiquitous large-scale sensing generates increased demands for scalability, prolonged network lifetime and reduced monetary cost, challenging existing WSN technologies to accommodate strict budget or energy constraints.

Scatter radio, i.e., communications by means of reflection [2], although dating back to 1948, has only recently emerged as a potential key-enabling technology for ubiquitous sensing. Scatter radio has been extensively utilized in radio frequency identification (RFID) systems for supply chain monitoring and object tracking. Rapid advances in sensor technology and the evolution of RFID systems has facilitated the integration of low-cost sensors with RFID technology [3], [4], giving rise to a new generation of low-cost and low-power WSNs that deviate from conventional sensor network wisdom.

Scatter radio achieves this by centrally generating a carrier wave that is used to simultaneously illuminate *multiple* tags/sensors. The tags do not actively radiate power but instead rely on the principle of *reflecting* the incident carrier signal while altering the physical properties of an antenna in a way that depends upon the data sensed. The benefit of such approach lies in the fact that the sensors/tags adhere to simpler radio frequency (RF) emitter designs, essentially consisting of a single RF transistor switch. This way, both monetary cost and energy requirements can be kept at relatively low levels, enabling dense large-scale sensor deployments that overcome many of the issues associated with conventional WSN systems. Furthermore, scatter radio can enable chip-less sensors with numerous applications - an example can be found in [5] and references therein.

Commercial RFID readers and passive (i.e., battery-less) tags/sensors typically lie at the heart of existing scatter radio sensing testbeds. Monostatic architectures are usually employed, where the transmit antenna generating the carrier as well as the receive antenna for demodulating reflected signal are part of the same equipment. However, monostatic architectures are characterized by the severe impact of the round-trip path loss since the carrier signal needs to propagate from the reader to the tag and subsequently be reflected back. In conjunction with passive tags, monostatic architectures offer limited communication ranges, on the order of a few meters (signal-to-noise ratio at the receiver drops at minimum with the fourth power of reader-to-tag distance [6]).

In monostatic architectures, examples of noncoherent receivers can be found in [3], [7] and examples of coherent receivers can be found for single-antenna readers in [8], [9] or multiple-antenna readers in [8]. For the coherent receivers, commercial RFID tags with FM0 line-coding and on-off keying (OOK) modulation were utilized and careful modeling of I and Q components of the received signal was exploited with zero-forcing [8] or maximum-likelihood (ML) [9] techniques.

Parts of this work have been submitted to IEEE International Conference on Communications (ICC), June 2015, London, UK. This work was supported by the ERC-04-BLASE project, executed in the context of the "Education & Lifelong Learning" Operational Program of the National Strategic Reference Framework (NSRF), General Secretariat for Research & Technology (GSRT), funded through European Union-European Social Fund and Greek national funds. Authors are with Telecom Lab, School of Electronic and Computer Engineering (ECE), Technical University of Crete, Chania 73100, Greece (Contact Prof. Aggelos Bletsas, e-mail: aggelos@telecom.tuc.gr, tel:+30-28210-37377, fax: +30-28210-37542).

However, the focus was on collision recovery at the physical layer (when more than one tag reflected simultaneously), rather than increasing communication range.

For increased communication ranges, *semi-passive* (i.e., energy-assisted) tags have been proven effective; such tags include an external energy source (e.g. battery) [3] or rely on energy harvesting techniques [10]–[12] but continue to employ reflection rather than active transmission. Such approach was followed in [3] which proposed battery-assisted tags, coupled with a monostatic architecture and offered detection algorithms for noncoherent minimum-shift keying (MSK) modulation at the tags. Such modulation allowed for simultaneous reflection of multiple tags without collision using simple frequency division multiplexing (FDM). Assuming very small bit rates - sufficient for sensing application where stable environmental conditions are monitored - the authors in [3] demonstrated extended tag-reader ranges on the order of 15m in an indoor scenario with as little as 7dBm transmit power and SDR techniques.

To further increase sensing/communication ranges, *bistatic* architectures have recently been proposed [7], [13], [14]. Bistatic setups are formed by dislocating the carrier signal generator from the reader, effectively addressing most of the drawbacks of monostatic architectures; multiple low-cost carrier emitters can be placed in a given area, forming cells where each emitter illuminates a different subset of tags. This way, the probability that a tag is placed close to a carrier emitter increases, offering potential link budget gains. Recently proposed *ambient* backscatter [15], where scatter radio terminals parasitically modulate information on top of a signal emitted from a distant TV station emitter, is also a promising case of bistatic scatter radio applications.

Bistatic scatter radio principles for low-bit rate sensing applications, in conjunction with FSK can naturally facilitate efficient multiple access schemes; each sensor/tag within a cell can be associated with a unique part of the spectrum, thus enabling FDM. Low cost carrier emitters can further utilize a time division multiplexing (TDM) scheme to mitigate interference among neighbouring cells. Demonstration of collision-free, multiple access with bistatic scatter radio principles and receiver-less environmental humidity sensors was recently offered in [16]. The authors networked a greenhouse with analog bistatic scatter radio principles and demonstrated the advantages and disadvantages of (bistatic) scatter radio technology. Given that the focus was on ultra-low cost, simple analog designs were exploited.

The complete bistatic scatter radio signal model with on-off keying (typically employed in commercial RFID systems), as well as FSK (ideal for the power-limited regime) was derived in [7], [13], [14]. The authors proposed noncoherent detectors for each modulation scheme and subsequently demonstrated experimental ranges on the order of 100 meters, using semi-passive tags in an outdoor scenario with 13dBm transmission power.

An additional approach towards range maximization relies on the use of channel codes (i.e., error-correction coding), which under certain conditions, exhibit vanishing probability of error as the codeword length, i.e., number of coded bits, goes to infinity. From a practical point of view, scatter radio cannot support such class of codes, due to limited tag processing and storage capabilities; error-correction codes of a) *short* codeword length and b) *low-complexity* encoding, appropriate for resource-constrained tags/sensors are strict design options.

Work in [17] first employed channel coding (i.e., error-correction) techniques, tailored to the noncoherent bistatic (uncoded) scatter radio setup of [7] to further increase communication ranges. The authors proposed low-complexity (small codeword length) encoding for adding redundancy to the information reflected by the tag; a near-optimal joint detection-decoding procedure was then proposed to exploit such redundancy for improved BER performance at the reader. Experimental results demonstrated range gains on the order of meters compared to the uncoded setup of [7].

This work further increases range coverage by developing novel *coherent* (instead of noncoherent) receivers for bistatic scatter radio and low-bit rate sensing appliations, extending recent work in [7]. Such task may seem formidable since (a) in the bistatic setup signals propagate over three different channels, as opposed to the single communication channel of conventional point-to-point communications and (b) scatter radio further complicates the problem by introducing additional design parameters (such as antenna structural mode, antenna reflection coefficients, scattering efficiency), which are generally unknown at the receiver. Despite the challenging nature of scatter radio, the proposed coherent receiver improves BER performance compared to state-of-the-art and specific analytical, simulation as well as experimental corroborating results are offered.

Furthermore, additional range gains are achieved by proposing specific short block-length cyclic channel codes. The scatter radio tag introduces redundancy to the reflected information (encoding) and the receiver/reader exploits such redundancy to improve BER performance (decoding). The proposed approach requires minimum encoding complexity at the tag (ideal for resource-constrained scatter radio tags), adheres to simple low-complexity decoding at the reader and achieves high-order signal diversity through appropriate low-complexity prepossessing.

More specifically, this work:

- Derives the optimal ML coherent detector for the bistatic scatter radio channel and provides a simple procedure to estimate the unknown (channel or microwave) parameters. The analytical error performance of the system is offered and losses due to imperfect channel estimation are analyzed.
- Proposes specific small codeword-length cyclic block codes with optimal (ML) low-complexity decoding. The structure of the specific class of codes is further exploited to perform low-complexity encoding, guaranteed to achieve high-order diversity.
- Experimentally validates the theoretical design and demonstrates extended tag-reader ranges on the order of 150 meters with as little as 20mW transmission power and omnidirectional antennas. It is experimentally verified that the proposed receivers offer range extension on the order of 10 meters compared to state-of-the-art

noncoherent receivers for bistatic scatter radio.

The rest of the work is organized as follows. Section II provides the system model and describes the utilized modulation scheme. Section III presents the full bistatic coherent reception scheme, as well as a simple approach to estimate channel parameters with the analytical bit error performance subsequently presented in Section IV. Specific short block length channel codes are incorporated in the coherent bistatic setup and the corresponding decoding procedure is offered in Section V. Detailed simulations as well as experimental results are given in Section VI corroborating the extended communication range capability of the proposed approach. Finally, the conclusion is offered in Section VII.

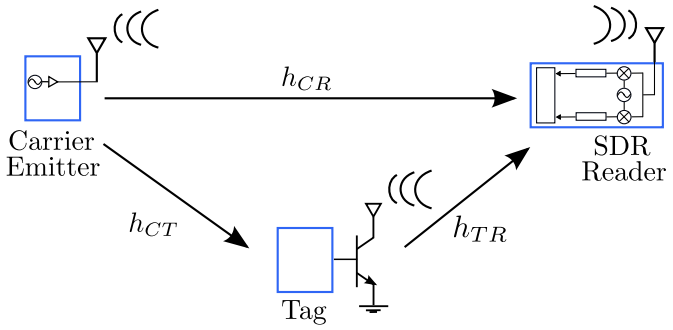

Fig. 1. Bistatic architecture system model: the carrier emitter is displaced from SDR reader and RF tag modulates the incident RF signal from the carrier emitter.

II. Signal Model and Modulation Scheme

The bistatic scatter radio architecture is employed [7], with a carrier emitter, a sensor/tag and a software-defined radio (SDR) reader, as depicted in Fig. 1. In contrast to conventional monostatic RFID systems, the carrier emitter is dislocated from the SDR reader and transmits a carrier at the ultra high frequency (UHF) band. The semi-passive sensor/tag performs binary modulation by switching its antenna load between two distinct values with different rates F_0 and F_1, corresponding to bit 0 and bit 1, respectively.[1] The carrier wave is then reflected with changed frequency and phase depending on the (modulating) antenna load of the tag.

Due to the relatively small communication bandwidth, i.e., low bit rate sensing applications, frequency non-selective fading is assumed. For flat fading, the baseband complex channel model for the three links (depicted in Fig. 1) during channel coherence time T_{coh}, is given by:

$$h_l = a_l e^{-j\phi_l}, \quad l \in \{\text{CR}, \text{CT}, \text{TR}\}, \tag{1}$$

where $a_{\text{CT}}, a_{\text{TR}}, a_{\text{CR}} \in \mathbb{R}_+$ denote the channel attenuation parameters and $\phi_{\text{CT}}, \phi_{\text{TR}}, \phi_{\text{CR}} \in (0, 2\pi)$ denote the corresponding phases due to signal propagation delay. The channel parameters $h_{\{\text{CT,TR,CR}\}}$ above are assumed circularly symmetric, complex Gaussians, with non-identical variances i.e., $h_l \sim \mathcal{CN}(0, \sigma_l^2), \quad l \in \{\text{CR}, \text{CT}, \text{TR}\}$. Additionally, the channel parameters are independent of each other and change independently every T_{coh}.

The carrier emitter transmits a continuous carrier of frequency F_{car} with complex baseband equivalent given by:

$$c(t) = \sqrt{2P_c} e^{-j(2\pi \Delta F t + \Delta\phi)}, \tag{2}$$

where ΔF and $\Delta\phi$ model the frequency and phase offset, respectively, between the carrier emitter and the SDR reader and P_c denotes the carrier transmission power.

The tag reflects the incident, attenuated and phase-rotated waveform $a_{\text{CT}} e^{-j\phi_{\text{CT}}} c(t)$. The reflected modulated waveform is further attenuated by a constant s, which depends on the tag inherent scattering efficiency.[2] The baseband scattered waveform can be written as:

$$x(t) = s u_i(t) a_{\text{CT}} e^{-j\phi_{\text{CT}}} c(t), \quad i \in \{0, 1\}. \tag{3}$$

For FSK modulation, waveform $u_i(t)$ (which corresponds to bit $b_i \in \{0, 1\}$) represents the fundamental frequency component of a 50% duty cycle square waveform of frequency F_i and random initial phase $\Phi_i \in [0, 2\pi)$:[3]

$$u_i(t) = u_0 + \frac{\Gamma_0 - \Gamma_1}{2} \frac{4}{\pi} \cos(2\pi F_i t + \Phi_i), \quad i \in \{0, 1\}, \tag{4}$$

where u_0 is a constant depending on the tag antenna structural mode A_s and the tag reflection coefficients Γ_0, Γ_1 [19].

For duration T of a single bit $b_i \in \{0, 1\}$, the received baseband signal at the SDR homodyne reader is given by the superposition of the carrier emitter sinusoid and the backscattered tag signal through channels h_{CR} and h_{TR}, respectively:

$$y(t) = a_{\text{CR}} e^{-j\phi_{\text{CR}}} c(t) + a_{\text{TR}} e^{-j\phi_{\text{TR}}} x(t) + n(t), \tag{5}$$

where $n(t)$ is a circularly symmetric, complex baseband additive Gaussian noise process with power spectral density (PSD):

$$S_{nn}(F) = \begin{cases} \frac{N_0}{2}, & |F| \leq W \\ 0, & \text{otherwise.} \end{cases} \tag{6}$$

Parameter W denotes the SDR reader receiving bandwidth. It is noted that the system model adopted from [7], has been extensively verified experimentally [13], [14], [16], [20], [21].

III. Receivers for Bistatic Scatter Radio Binary FSK (BFSK)

By substituting Eqs. (2)–(4) in Eq. (5), the received baseband signal at the SDR reader for duration T of a single bit

[1] Additional termination loads can facilitate M-ary modulations, as experimentally shown in [18].

[2] When passive tag/sensors are used with RF energy harvesting, the amount of scattered power may depend on the amount of harvested power, which in turn depends on the RF harvester efficiency and overall tag hardware architecture. Here, we have not utilized passive tags or RF energy harvesting, but instead, semi-passive tags are assumed, where energy may come from battery or other energy harvesting solar or thermal or chemical sources.

[3] It can be shown that the fundamental frequency component holds $\approx 80\%$ of the total power of the 50% duty cycle square pulse [3].

$b_i \in \{0,1\}$ can be written as:

$$y(t) = \underbrace{\left(\sqrt{2P_c}e^{-j\Delta\phi}\left(a_{\rm CR}e^{-j\phi_{\rm CR}} + sa_{\rm CT}a_{\rm TR}u_0e^{-j(\phi_{\rm CT}+\phi_{\rm TR})}\right)\right.}_{\text{DC term}}$$
$$\left. + m_{\rm CTR}e^{-j\phi_{\rm CTR}}\cos(2\pi F_i t + \Phi_i)\right) \times e^{-j2\pi\Delta F t} + n(t), \quad (7)$$

where the following simplified notation has been used:

$$\phi_{\rm CTR} = \phi_{\rm CT} + \phi_{\rm TR} + \Delta\phi + \angle(\Gamma_0 - \Gamma_1),$$
$$m_{\rm CTR} = \sqrt{2P_c}|\Gamma_0 - \Gamma_1|a_{\rm CT}a_{\rm TR}\frac{2}{\pi}s. \quad (8)$$

The carrier frequency offset (CFO) can be directly estimated and subsequently compensated using standard periodogram-based estimation techniques, as in [7]. The periodogram estimate coincides with the maximum-likelihood estimate (MLE), which asymptotically offers mean-squared error (MSE) that decays with the cubic power of the number of utilized samples [22, pp. 542].

The DC term, which conveys no bit information, can be eliminated by estimation and removal of the received signal's mean value $\mathbb{E}\{y(t)\}$. Both CFO and DC term estimation require strong carrier and tag signals; design parameters relevant to such requirement (e.g. tag antenna structural mode) are discussed in [7]. The received signal waveform over one bit period T is then given by:

$$y(t) = h_{\rm CTR}\cos(2\pi F_i t + \Phi_i) + n(t) \quad (9)$$

or equivalently, by:

$$y(t) = \frac{h_{\rm CTR}}{2}\left(e^{j(2\pi F_i t + \Phi_i)} + e^{-j(2\pi F_i t + \Phi_i)}\right) + n(t), \quad (10)$$

with

$$h_{\rm CTR} = m_{\rm CTR}e^{-j\phi_{\rm CTR}}. \quad (11)$$

The fading model in (11) is equivalent to a special case of the dyadic backscatter channel first presented in [23].

Eq. (10) reveals *two* subcarriers for each frequency F_i (due to the cosine term), one at the positive semiaxis (F_i) and one at the negative ($-F_i$). That is due to the fact that the tag/sensor modulates the carrier directly at passband, through reflection (of the carrier), explained above. In contrast, for a classic FSK transmitter, only one subcarrier appears for each frequency and the optimum FSK receiver correlates the received signal against frequencies F_0 and F_1 for signal detection [24, pp. 178]. If the same receiver was utilized for the bistatic FSK signal model above, the subcarriers at frequencies $-F_0$ and $-F_1$ would not be considered, resulting in a 3dB performance loss. Evidently, a classic FSK receiver is not directly applicable in such scatter radio setup and work in [7] provided the appropriate *noncoherent* design.

The following theorem assists the design of *coherent* reception, since all unknown (at the receiver) complex channel gains and synchronization parameters, including emitter-to-tag link's, are concentrated to a *single* 4×1 complex vector:

Theorem 1: The complex vector baseband equivalent of the received signal of Eq. (10), for duration T of a single bit $b_i \in \{0,1\}$, is given by:

$$\mathbf{r} = \mathbf{h} \odot \mathbf{s}_{b_i} + \mathbf{n}, \quad (12)$$

where $\odot$ denotes the component-wise (Hadamard) product and elements of the corresponding vectors are given by:

$$\begin{bmatrix} r_0^+ \\ r_0^- \\ r_1^+ \\ r_1^- \end{bmatrix} = \begin{bmatrix} \frac{\sqrt{T}h_{\rm CTR}}{2}e^{+j\Phi_0} \\ \frac{\sqrt{T}h_{\rm CTR}}{2}e^{-j\Phi_0} \\ \frac{\sqrt{T}h_{\rm CTR}}{2}e^{+j\Phi_1} \\ \frac{\sqrt{T}h_{\rm CTR}}{2}e^{-j\Phi_1} \end{bmatrix} \odot \begin{bmatrix} (1-b_i) \\ (1-b_i) \\ b_i \\ b_i \end{bmatrix} + \begin{bmatrix} n_0^+ \\ n_0^- \\ n_1^+ \\ n_1^- \end{bmatrix}, \quad (13)$$

where $\mathbf{s}_{b_i} = [1\ 1\ 0\ 0]^T$ for $b_i = 0$ and $\mathbf{s}_{b_i} = [0\ 0\ 1\ 1]^T$ for $b_i = 1$. For $F_i + 20/T \ll W$, the random vector $\mathbf{n} \sim \mathcal{CN}\left(\mathbf{0}, \frac{N_0}{2}\mathbf{I}_4\right)$.

Proof: in Appendix I. ■

The *average* received signal-to-noise ratio (SNR) is defined as:

$$\overline{\rm SNR} \triangleq \frac{\mathbb{E}\{\mathrm{E}_b\}}{N_0/2} = \frac{(8/\pi^2)|\Gamma_0 - \Gamma_1|^2 s^2 P_c \mathbb{E}\{(a_{\rm CT})^2\}\mathbb{E}\{(a_{\rm TR})^2\}T}{N_0}$$
$$= \frac{(8/\pi^2)|\Gamma_0 - \Gamma_1|^2 s^2 P_c \sigma_{\rm CT}^2 \sigma_{\rm TR}^2 T}{N_0}, \quad (14)$$

where E_b is the instantaneous energy per bit.

A. Noncoherent Detection for Bistatic BFSK Modulation [7]

For noncoherent detection and equiprobable signals, the optimal (in the sense of minimizing the probability of error) detection rule is given by:

$$b_i^{\rm ML} = \underset{b_i\in\{0,1\}}{\rm argmax}\ p(\mathbf{r}|\mathbf{s}_{b_i}) = \underset{b_i\in\{0,1\}}{\rm argmax} \int p(\mathbf{r}|\mathbf{s}_{b_i}, \mathbf{h})p(\mathbf{h})d\mathbf{h}, \quad (15)$$

where in the last relation, averaging is performed over random parameter vector $\mathbf{h}$.

There exists no closed form solution for the expression of Eq. (15). As a practical alternative, the authors in [7] and [17] consider instead a heuristic approximation to the above detection rule. More specifically:

$$z_0 \triangleq |r_0^+|^2 + |r_0^-|^2 \overset{\text{bit } 0}{\geq} |r_1^+|^2 + |r_1^-|^2 \triangleq z_1. \quad (16)$$

Subsequent work [25] showed that the detection rule in (16) is a result of a composite hypothesis testing. It is observed that the above detection rule does not require the channel statistics and is solely based on the received information.

B. Coherent Detection for Bistatic BFSK Modulation

Assuming available channel estimate $\widehat{\mathbf{h}}$ and equiprobable signaling, the optimal (in the sense of minimizing the probability of error) detection rule is given by:

$$b_i^{\rm ML} = \underset{b_i\in\{0,1\}}{\rm argmax}\ p(\mathbf{r}|\mathbf{s}_{b_i}, \widehat{\mathbf{h}})$$
$$= \underset{b_i\in\{0,1\}}{\rm argmax}\ \exp\left\{-\frac{2}{N_0}\left\|\mathbf{r} - \widehat{\mathbf{h}} \odot \mathbf{s}_{b_i}\right\|_2^2\right\}$$
$$= \underset{b_i\in\{0,1\}}{\rm argmin}\ \left\|\mathbf{r} - \widehat{\mathbf{h}} \odot \mathbf{s}_{b_i}\right\|_2^2$$
$$= \underset{b_i\in\{0,1\}}{\rm argmin}\ -\Re\left(\left(\widehat{\mathbf{h}} \odot \mathbf{s}_{b_i}\right)^H \mathbf{r}\right), \quad (17)$$

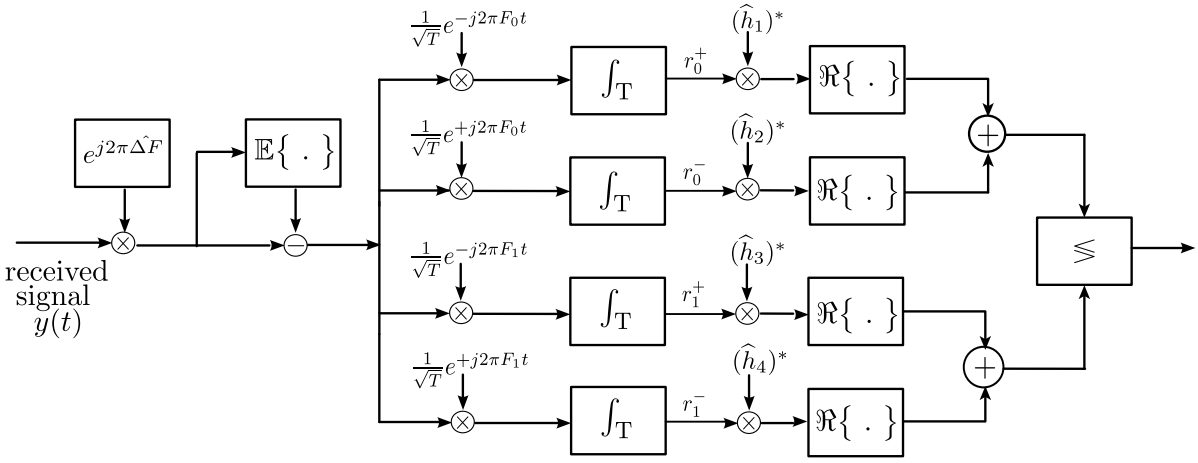

Fig. 2. The structure of the coherent correlation receiver for bistatic scatter radio with 4 correlators and 4 complex channel gains (2 for each FSK frequency).

where superscript $()^H$ denotes the conjugate-transpose of a matrix or vector. After elementary calculations, the above decision rule can be written as:

$$\Re\left((\widehat{h}_1)^*\ r_0^+ + (\widehat{h}_2)^*\ r_0^-\right) \overset{\text{bit 0}}{\geq} \Re\left((\widehat{h}_3)^*\ r_1^+ + (\widehat{h}_4)^*\ r_1^-\right), \tag{18}$$

where $\widehat{\mathbf{h}} = \left[\widehat{h}_1\ \ \widehat{h}_2\ \ \widehat{h}_3\ \ \widehat{h}_4\right]^T$. The coherent receiver is depicted in Fig. 2 and employs the above detection rule.

C. Channel Estimation

To coherently detect the received signal by Eq. (18), both the compound channel h_{CTR} as well as the random phases $\Phi_i,\ i \in \{0,1\}$ need to be estimated. A training signal, a priori known at the receiver, is periodically transmitted and the receiver then employs an optimization procedure based on least-squares (LS) estimation. Such pilot signal could be the preamble, typically used for packet and/or symbol synchronization.

More specifically, once during the channel coherence time T_{coh}, N_{tr} training bits $\{b_{i_{\text{tr}}}\}$, $i_{\text{tr}} = 1, \ldots, N_{\text{tr}}$, are transmitted by the tag. After demodulation, CFO estimation and DC blocking, the vector representation of the received training signal over one bit period T is given by Eq. (12):

$$\mathbf{r}_{i_{\text{tr}}} = \mathbf{h} \odot \mathbf{s}_{b_{i_{\text{tr}}}} + \mathbf{n}_{i_{\text{tr}}}, \tag{19}$$

which can also be written as:

$$\mathbf{r}_{i_{\text{tr}}} = \mathbf{V}_{b_{i_{\text{tr}}}}\mathbf{h} + \mathbf{n}_{i_{\text{tr}}}, \tag{20}$$

with

$$\mathbf{V}_{b_{i_{\text{tr}}}} = \left[(1-b_{i_{\text{tr}}})\mathbf{e}_1 \quad (1-b_{i_{\text{tr}}})\mathbf{e}_2 \quad b_{i_{\text{tr}}}\mathbf{e}_3 \quad b_{i_{\text{tr}}}\mathbf{e}_4\right] \in \mathbb{C}^{4\times 4}, \tag{21}$$

where $\mathbf{e}_k,\ k = 1, \ldots, 4$, denotes the k-th column of the $\mathbf{I}_4$ identity matrix.

Next, by the column-wise concatenation of the vector representations of the N_{tr} bits in the training sequence, the receiver creates vector $\mathbf{y} \in \mathbb{C}^{4N_{\text{tr}}}$:

$$\mathbf{y} = \begin{bmatrix} \mathbf{r}_1 \\ \mathbf{r}_2 \\ \vdots \\ \mathbf{r}_{N_{\text{tr}}} \end{bmatrix} = \begin{bmatrix} \mathbf{V}_{b_1} \\ \mathbf{V}_{b_2} \\ \vdots \\ \mathbf{V}_{b_{N_{\text{tr}}}} \end{bmatrix} \mathbf{h} + \begin{bmatrix} \mathbf{n}_1 \\ \mathbf{n}_2 \\ \vdots \\ \mathbf{n}_{N_{\text{tr}}} \end{bmatrix} = \mathbf{A}\mathbf{h} + \mathbf{n}. \tag{22}$$

To jointly estimate the compound channel h_{CTR} and phases $\Phi_i, i \in \{0,1\}$, the receiver solves the LS problem:

$$\begin{bmatrix} \widehat{h}_1 \\ \widehat{h}_2 \\ \widehat{h}_3 \\ \widehat{h}_4 \end{bmatrix} = \widehat{\mathbf{h}} \triangleq \mathbf{h}^{\text{LS}} = \underset{\mathbf{h}\in\mathbb{C}^4}{\operatorname{argmin}} \|\mathbf{y} - \mathbf{A}\mathbf{h}\|_2^2, \tag{23}$$

It is noted that while the aforementioned LS approach ignores the dependencies in vector $\mathbf{h}$, it adheres to a simple non-iterative solution. Taking the derivative $\frac{d}{d\mathbf{h}}\left(\|\mathbf{y} - \mathbf{A}\mathbf{h}\|_2^2\right)$ and setting it to zero offers [26, pp. 280]:

$$\mathbf{h}^{\text{LS}} = \left(\mathbf{A}^H\mathbf{A}\right)^{-1}\mathbf{A}^H\mathbf{y}. \tag{24}$$

For noise $\mathbf{n}$ white and complex Gaussian, it is easy to see that the above solution $\widehat{\mathbf{h}}$ is also the ML estimate of the channel $\mathbf{h}$.

IV. Probability of Error for Coherent Bistatic BFSK

A. Conditional Probability of Error

Assuming equiprobable signaling and due to the symmetry of the constellation, it can be easily shown that:

$$p(e|\mathbf{h}) = p(e|h_{\mathrm{CTR}}) = Q\left(\frac{\sqrt{T}|h_{\mathrm{CTR}}|}{\sqrt{N_0}}\right). \tag{25}$$

Substituting $|h_{\mathrm{CTR}}| = m_{\mathrm{CTR}} = \sqrt{2P_c}|\Gamma_0 - \Gamma_1|a_{\mathrm{CT}}a_{\mathrm{TR}}\frac{2}{\pi}s$ by Eq. (8), the conditional probability of error can be expressed as a function of the average received SNR, $\overline{\mathrm{SNR}}$:

$$p(e|h_{\mathrm{CTR}}) = p(e|a_{\mathrm{CT}}, a_{\mathrm{TR}}) = Q\left(\frac{a_{\mathrm{CT}}}{\sigma_{\mathrm{CT}}}\frac{a_{\mathrm{TR}}}{\sigma_{\mathrm{TR}}}\sqrt{\overline{\mathrm{SNR}}}\right). \tag{26}$$

B. Probability of Error

***Theorem** 2:* The probability of error is offered by averaging over h_{CTR} and is given by:

$$p(e) = \mathop{\mathbb{E}}_{h_{\mathrm{CTR}}}\{p(e|h_{\mathrm{CTR}})\} = \mathop{\mathbb{E}}_{a_{\mathrm{CT}}}\left\{\mathop{\mathbb{E}}_{a_{\mathrm{TR}}}\{p(e|a_{\mathrm{CT}}, a_{\mathrm{TR}})\}\right\} = \frac{1}{2} - \frac{\sqrt{\pi}}{4}\mathrm{U}\left(\frac{1}{2}, 0, \frac{2}{\overline{\mathrm{SNR}}}\right), \quad (27)$$

where $\mathrm{U}(a, b, z)$ denotes the *confluent hypergeometric* U function (Eq. (48) in Appendix II).

Proof: in Appendix II. ∎

V. Channel Codes and Signal Diversity

In the context of bistatic scatter radio, application of channel codes is especially challenging due to hard design constraints; scatter radio tags are inherently resource-constrained in terms of computation speed (due to limited clock frequency), resolution (due to typically 8- or 16-bit architecture) and memory and thus, any type of processing must be computationally affordable. This means that coding schemes capable of approaching the theoretical limits of performance (capacity approaching codes) are not applicable due to non-negligible encoding requirements (e.g. memory). In addition, decoding at the receiver should be also low-complexity; if not, decoding-induced delays would limit the potential number of tags served by a single receiver.

A. Encoding At The Tags

The objective of encoding, performed directly by the scatter radio tag/sensor, is to introduce redundancy, by mapping a sequence of k information bits (denoted as vector $\mathbf{m} \in \{0,1\}^k$) to $n \geq k$ *coded* bits (denoted as vector $\mathbf{c} \in \{0,1\}^n$). The collection of all such 2^k possible n-dimensional vectors, i.e., the code, is usually denoted as $\mathcal{C}(n,k)$. The particular class of *cyclic* codes [27, Sec. 8.1] offers efficient encoding by associating vectors with polynomials: any vector $\mathbf{v} = (v_0, v_1, \ldots, v_{n-1}) \in \{0,1\}^n$ is represented as polynomial $v(x) = v_0 + v_1 x + \ldots + v_{n-1}x^{n-1}$ with an one-to-one correspondence. The main theorem of cyclic codes then states that for code $\mathcal{C}(n,k)$ there exists a unique monic[4] *generator* polynomial $g(x)$ of degree $n-k$ such that every codeword polynomial $c(x)$ can be expressed as a multiple of this generator:

$$c(x) = m(x)g(x). \quad (28)$$

Eq. (28) represents the encoding operation that maps k information bits to n coded bits. This operation can be performed efficiently with a shift register of $n-k$ memory elements, a process referred to as *shift register encoding* [27, Sec. 8.2]. The latter is ideal for ultra low-cost, low-power micro-controller based scatter-radio tags, such as the ones utilized in this work. It is emphasized that the tags are memory-constrained also, therefore the values of k and n should be kept relatively small.

[4]A monic polynomial is a polynomial whose non-zero coefficient of highest degree is equal to 1.

B. ML Coherent Soft-Decision Decoding for Bistatic BFSK

Decoding refers to the process of exploiting the code information redundancy, by performing detection over a *sequence* of n bits belonging to the same code. More specifically, let $\mathcal{C}$ be the code and let codeword

$$\mathbf{c} = [c_1 \;\; c_2 \ldots \;\; c_n] \in \mathcal{C} \quad (29)$$

be reflected by the tag. Assuming that the codeword length is strictly smaller (in time duration) than the channel coherence time, by Eq. (12) the SDR reader receives:

$$\mathbf{r}_i = \mathbf{h} \odot \mathbf{s}_{c_i} + \mathbf{n}_i, \quad i = 1, \ldots, n, \quad (30)$$

with $\mathbf{s}_{c_i} = \begin{bmatrix} 1-c_i & 1-c_i & c_i & c_i \end{bmatrix}^T$.

Then, assuming compound channel estimate $\widehat{\mathbf{h}}$ and equiprobable signaling, the optimal (in the sense of minimizing the probability of decoding error) decoding rule is given by:

$$\begin{aligned}
\mathbf{c}^{\mathrm{ML}} &= \mathop{\mathrm{argmax}}_{\mathbf{c}\in\mathcal{C}} p([\mathbf{r}_1 \;\; \mathbf{r}_2 \;\; \ldots \;\; \mathbf{r}_n] \,|\mathbf{c}, \widehat{\mathbf{h}}) \\
&= \mathop{\mathrm{argmax}}_{\mathbf{c}\in\mathcal{C}} \prod_{i=1}^{n} p(\mathbf{r}_i|c_i, \widehat{\mathbf{h}}) \\
&= \mathop{\mathrm{argmax}}_{\mathbf{c}\in\mathcal{C}} \prod_{i=1}^{n} \exp\left\{-\frac{2}{N_0}\left\|\mathbf{r}_i - \widehat{\mathbf{h}} \odot \mathbf{s}_{c_i}\right\|_2^2\right\} \\
&= \mathop{\mathrm{argmin}}_{\mathbf{c}\in\mathcal{C}} \sum_{i=1}^{n} \left\|\mathbf{r}_i - \widehat{\mathbf{h}} \odot \mathbf{s}_{c_i}\right\|_2^2 \\
&= \mathop{\mathrm{argmax}}_{\mathbf{c}\in\mathcal{C}} \Re\left(\sum_{i=1}^{n}\left(\widehat{\mathbf{h}} \odot \mathbf{s}_{c_i}\right)^H \mathbf{r}_i\right).
\end{aligned} \quad (31)$$

The ML decoder is optimal but has complexity exponential in the code dimension k; for memory-constrained scatter radio tags/sensors, value k is necessarily small and thus, the ML decoder is a practical option.

C. Signal Diversity Through Coding

In fading environments, the errors usually occur in bursts when the channel is in a deep fade; for bistatic scatter radio the probability of such deep fade is even larger due to the product of channel gains h_{CT} and h_{TR}. When the channel is in a deep fade, the code-bits of a specific codeword fade simultaneously and a (short block length) channel code is not powerful enough to correct the sheer amount of reception errors.

Signal diversity through channel coding is achieved through the interleaving technique, designed such that burst errors affect bits of different codewords rather than consecutive bits of the same codeword. The tag encodes and subsequently stores a block of D codewords in a $D \times n$ matrix and the information is then transmitted column-wise. Parameter D is called the interleaving depth of interleaver. The receiver stores the $D \times n$ received symbols by writing the columns of a matrix and performs ML decoding row-wise. This way, the receiver effectively decodes symbol sequences, which correspond to codewords with coded bits experiencing independent fading.

The interleaving technique has the effect of considerably reducing the probability that all code-bits will fade simultaneously. The following theorem shows that the fully interleaved

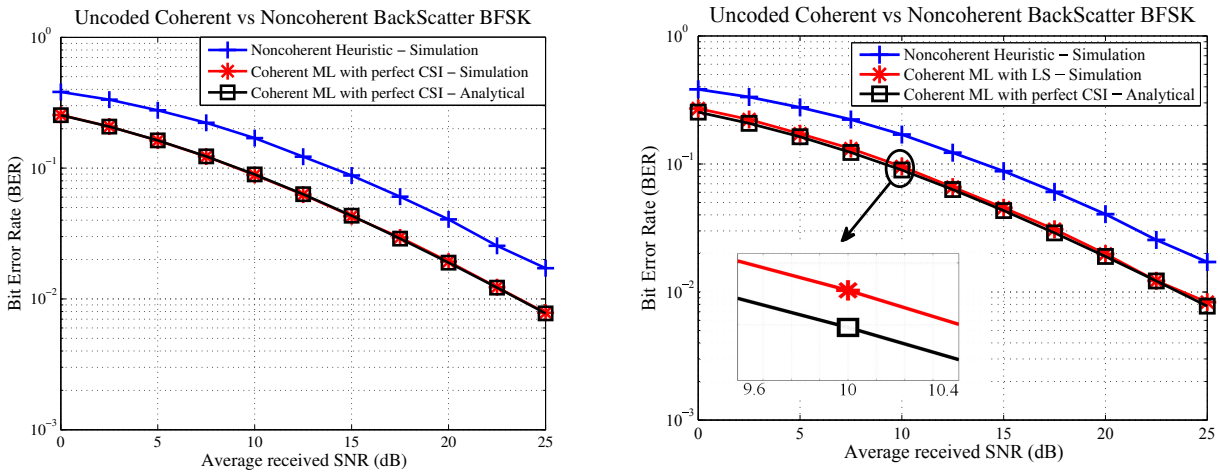

Fig. 3. Bit error rate (BER) performance as a function of the average received SNR for the uncoded bistatic setup, with coherent and noncoherent receivers.

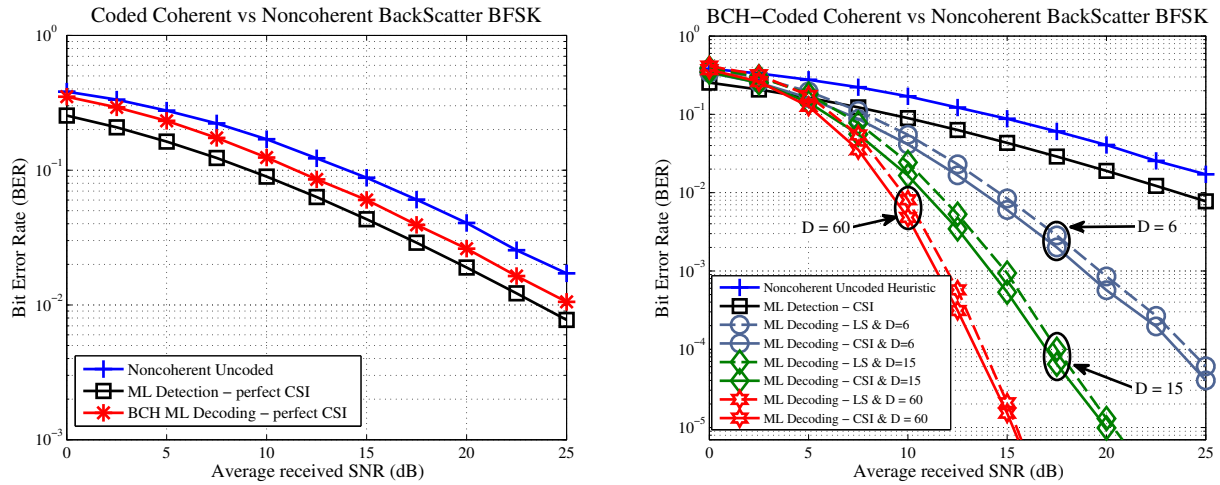

Fig. 4. Bit error rate (BER) performance as a function of the average received SNR for the coded bistatic setup, utilizing the cyclic $\mathcal{C}(31, 11)$ BCH code. Left: Due to severe fading events, coherent detection outperforms ML decoding. Right: Bit interleaving can effectively mitigate the degradation due to fading and improves performance as the interleaving depth increases.

system under ML decoding can achieve diversity order $d_{\min}$, where $d_{\min}$ denotes the minimum distance of the code.[5]

***Theorem** 3:* Bistatic scatter radio system under ML decoding with full interleaving, i.e., $T_{\text{coh}} = (D + N_{\text{tr}})T$, achieves diversity order $d_{\min}$.

Proof: in Appendix III. ∎

However, the interleaving technique introduces delay and requires additonal memory, since both the scatter radio tag/sensor, as well as the receiver process a block of D codewords upon transmission and reception, respectively. Since the tag/sensor is equipped with limited memory, the interleaving technique as presented above may be a practical option only for relatively small values of D.

A more sophisticated method for achieving diversity is based on taking advantage of the mathematical structure of cyclic codes to reduce memory requirements. If $\mathcal{C}(n, k)$ is cyclic code with minimum distance $d_{\min}$, then interleaving $\mathcal{C}$ to depth D produces a new code $\mathcal{C}^D(Dn, Dk)$. The new code is called an *interleaved* code, and it can be shown [27, Sec. 8.4, Theorem 8.12] that the resulting code is cyclic and maintains a minimum distance of $d_{\min}$. If $g(x)$ is the generator of the original code, then $g(x^D)$ generates the interleaved code. Therefore, the tag/sensor can readily generate the interleaved sequence with a shift register encoder of $(n - k)D$ memory elements, as opposed to processing D blocks of n bits each.

[5]The minimum distance $d_{\min}$ of a code $\mathcal{C}$ is the smallest Hamming weight (i.e., the number of non-zero components) of any non-zero codeword in $\mathcal{C}$.

VI. Numerical Results

A. Uncoded BER Performance

Fig. 3 illustrates bit error rate (BER) performance as a function of the average received SNR for the uncoded bistatic setup of Fig. 1, where each channel link suffers from Rayleigh fading, i.e., $\{h_{\text{CT}}, h_{\text{TR}}, h_{\text{CR}}\} \sim \mathcal{CN}(0, 1)$. For the uncoded case, the channel coherence time is assumed to span a limited number of 200 bits during which $N_{\text{tr}} = 40$ training bits are utilized for solving the LS problem (23) and $N = 160$ bits carry useful information. It is assumed that the receiver synchronizes perfectly using the training bits and estimates the carrier frequency offset without error.

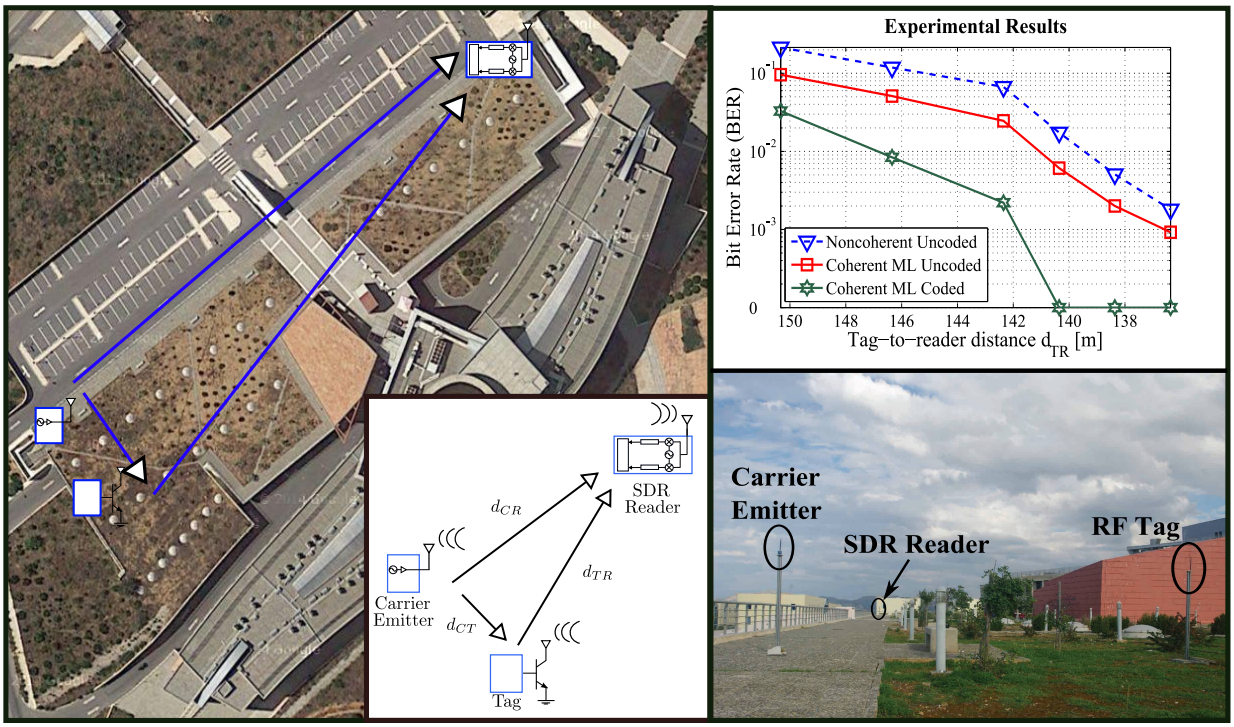

Fig. 5. Bistatic experimental setup panoramic view (left), bistatic experimental setup normal view (right-downwards) and the experimental BER plots (right-upwards). Carrier emitter, RF tag and software-defined radio are placed in a triangular topology on an open field. The distance between carrier emitter and RF tag is set to $d_{\mathrm{CT}} = 10$ meters.

Fig. 3-left depicts the analytical error rate performance of coherent detection given by Eq. (27), as well as the performance of coherent detection assuming perfect channel state information (CSI). It can be seen that analysis BER of Eq. (27) perfectly matches with simulation. Evidently, with perfect CSI the coherent detector demonstrates superior BER performance compared to the noncoherent detector with a performance gap of approximately 5dB at BER = 10%. In practice however, the proposed receiver estimates the channel characteristics with the LS approach of (23) and imperfect estimation causes less than 1dB degradation compared to the ideal (i.e., perfect CSI) case, as seen in Fig. 3-right. Therefore, despite estimation errors the proposed receiver offers a 4.6dB performance gain at target BER = 10% compared to the state-of-the-art noncoherent bistatic receiver of [7], at the expense of utilizing a small number of bits for channel estimation.

B. Coded BER Performance

Fig. 4 considers the use of a small block-length cyclic code, the BCH (31,11) channel code with generator found in [27]. For the coded case, the channel coherence time is assumed to span a limited number of 100 bits with $N_{\mathrm{tr}} = 40$ bits used for channel estimation. Regardless of the specific channel code employed, any given codeword contains $n-k$ redundant bits, used to correct errors occurring during transmission. An energy budget which allocates $\mathcal{E}_b$ Joules/bit for the k bits of uncoded data must spread that energy over the n bits of coded data, so that *total* energy between the coded and the uncoded scenario is kept constant:

$$n\mathcal{E}_b^{'} = k\mathcal{E}_b \Longrightarrow \mathcal{E}_b^{'} = \frac{k}{n}\mathcal{E}_b. \tag{32}$$

Specifically, for the considered BCH (31,11) code in Fig. 4, the energy per coded bit is $\mathcal{E}_b^{'} = \frac{11}{31}\mathcal{E}_b$.

Fig. 4-left depicts the BER performance of coherent ML decoding with the BCH (31,11) code assuming perfect channel estimation. It can be seen that the use of a channel code degrades performance compared to coherent detection. Such result can be explained by the fact that the compound channel h_{CTR} increases the probability of a deep fading event; the limited error correction capability of the utilized code cannot overcome the frequent deep-fading events. To bypass this issue, the interleaving technique of Sec. V is utilized.

Fig. 4-right depicts the BER of interleaved coherent ML decoding with the BCH (31,11) code assuming perfect channel estimation (labelled as CSI) and imperfect channel estimation with LS (labelled as LS). It can be observed that increasing the interleaving depth D offers tremendous performance gains. That is due to the fact that for fixed coherence time and increased D, the transmitted coded bits experience independent channel realizations and thus, channel diversity is also offered. Specifically, at BER $= 1\%$ the depth-6 interleaved BCH (31,11) code offers a coding gain of 9.8dB with perfect CSI and coding gain of 9dB with imperfect CSI, while depth-15 interleaved BCH code offers a coding gain of 12.8dB with perfect CSI and coding gain of 12.2dB with imperfect CSI, compared to coherent detection. Similarly, comparing to coherent detection, the depth-60 interleaved BCH code results in a 14.6dB coding gain with perfect CSI and coding gain of 14dB

TABLE I
EXPERIMENTAL SETUP PARAMETERS

SDR Noise Figure (Nominal Value)	8dB
SDR Digital Receive Bandwidth (W)	500kHz
Maximum SDR Analog Filter Bandwidth	30MHz
SDR Sampling Rate	10^6samples/sec
Carrier Emitter Power (P_c)	13dBm
Carrier Frequency (F_{car})	868MHz
Carrier Emitter Clock Frequency (Nominal Value)	24.5MHz
Carrier Emitter Clock Accuracy	$\pm 2\%$
Tag Transmission Rate	1kbps
Tag Sub-frequency F_0	125kHz
Tag Sub-frequency F_1	250kHz
Tag (External) Clock Frequency (Nominal Value)	24.5MHz
Tag (External) Clock Accuracy	$\pm$30ppm
Height of Antennas	1.70m
Type of Antennas	Monopoles
Antenna Gain (Nominal Value)	2.15dBi

with imperfect CSI. Since the performance gap between the coherent and the noncoherent detector is approximately 4dB at BER $= 1\%$, the proposed coherent decoder outperforms the noncoherent detector by 18dB assuming $D = 60$ and LS channel estimation.

C. Outdoor Experimental Results: Achieved Bistatic Ranges

Range measurements were conducted outdoors with the experimental setup of Fig. 5-left. A carrier emitter was set to transmit a carrier wave of frequency 868MHz with 13dBm transmit power. A custom, 8-bit microcontroller-based, semi-passive scatter radio tag was used to modulate at rate 1kbps, with FSK, as presented in Sec. II. A USRP-2 SDR with Flex-900 front-end radio card was utilized as the receiver, connected to a laptop running custom receiver scripts. Table I summarizes the experimental setup parameters utilized for the experimental measurements. Due to relative static environment (Fig. 5) channel coherence times 50 to 100msec were observed during the experimental results.

A packet of 30 training bits (known to receiver for synchronization and channel estimation for the coherent case) plus 31 bits corresponding to a BCH(31,11) codeword was utilized. Bit-wise detection using (18) was performed for the uncoded scenario while for the coded case the decoding rule of (31) was employed. It is noted that the encoding-decoding process does not utilize the interleaving technique. To maximize the achievable ranges, no energy budget was assumed and therefore the use of channel codes improves performance at the cost of rate reduction. In all considered scenarios, periodogram-based CFO estimation is utilized. In our implementation the entire received signal is employed to estimate the CFO. Synchronization was performed by correlating the received signal with the known training signal (preamble).

Fig. 5-right upwards offers the experimental BER as a function of the tag-to-reader distance for the experimental setup of Fig. 5-left. It can be observed that with a carrier-to-tag distance of $d_{\text{CT}} = 10$m, both coherent and noncoherent uncoded receivers achieve ranges on the order of 145m with BER $\leq 10\%$, corroborating the idea of bistatic scatter radio for increased-range sensing applications. It is emphasized that the reported BER on the order of 1%–5% is acceptable for the considered low bit-rate sensing applications. More importantly, it is found that the offered tag-to-reader ranges for BER on the order of 1%–5%, can be increased by at least 2-5 meters (compared to the noncoherent case) using the proposed coherent receiver or by 8-10 meters using the proposed low-complexity cyclic channel codes, in conjunction with the proposed decoding procedure.

VII. CONCLUSIONS

This work proposed the first coherent reception algorithm for the bistatic scatter radio channel. Even though the bistatic setup in conjunction with scatter radio introduces multiple unknown channel and microwave scatter radio parameters, this work provided a simple solution for bit error rate reduction or equivalently range increase. Simple short block length cyclic channel codes were further exploited, with simple low-complexity encoding implemented directly at the scatter radio tags and low-complexity ML decoding at the reader. The theoretical design was validated through both simulation and experimental results, with significant theoretical gains and range extension of 10 meters, compared to state-of-the-art non-coherent bistatic scatter radio receivers. Even though coherent detection/decoding for the bistatic scatter radio channel is by itself a great challenge, this work provided a simple solution that could expedite the adoption of scatter radio for large scale and ultra low-cost, ubiquitous sensor network applications.

ACKNOWLEDGMENTS

The authors would like to thank G. Theodorakis, K. Tzedaki, K. Tountas, E. Kampianakis, N. Kargas, S. Assimonis, N. Mitianoudis, D. Ntilis, C. Konstantopoulos and A. Deligiannakis for their assistance in various stages of this work.

APPENDIX I

Proof of Theorem 1: The received signal of Eq. (9) is the sum of two complex exponentials of frequencies $\pm F_i$ and unknown phases $(\pm\Phi_i - \phi_{\text{CTR}})$, $i \in \{0, 1\}$. Under the orthogonality criterion for noncoherent FSK:

$$|F_1 - F_0| = \frac{k}{T}, \quad k \in \mathbb{N}, \tag{33}$$

and the fact that $F_i \gg \frac{1}{T}$, $i \in \{0, 1\}$, any two exponentials of time duration T and frequencies $\pm F_0$, $\pm F_1$ will be orthogonal:

$$\left\langle e^{+j2\pi(F_i)t}, e^{+j2\pi(F_k)t} \right\rangle \triangleq \int_T e^{+j2\pi F_i t} \left(e^{+j2\pi F_k t}\right)^* dt = \begin{cases} T, & F_i = F_k, \\ 0, & F_i \neq F_k, \end{cases} \quad k, i \in \{0, 1\}, \tag{34}$$

where the subscript T in the integral denotes that integration is performed over one symbol (bit) period. Consequently, the set of exponentials of time duration T and frequencies $\pm F_0$, $\pm F_1$, normalized by $\sqrt{T}$, constitute an orthonormal basis [24,

pp. 30] that can be used for expansion of the received signal of Eq. (9).

Using each of the four basis functions, the noiseless random process $s(t,\Phi_i,h_{\rm CTR})=h_{\rm CTR}\cdot\cos(2\pi F_i t+\Phi_i)$ of Eq. (9) can be expanded as:

$$\begin{aligned}&\left\langle s(t,\Phi_i,h_{\rm CTR}),\frac{1}{\sqrt{T}}e^{+j2\pi F_0 t}\right\rangle\\&=\int_T h_{\rm CTR}\cos(2\pi F_i t+\Phi_i)\left(\frac{1}{\sqrt{T}}e^{+j2\pi F_0 t}\right)^* dt\\&=\int_T\frac{h_{\rm CTR}}{2\sqrt{T}}\left(e^{j(2\pi F_i t+\Phi_i)}+e^{-j(2\pi F_i t+\Phi_i)}\right)\left(e^{-j2\pi F_0 t}\right)dt\\&=\int_T\frac{h_{\rm CTR}}{2\sqrt{T}}e^{j(2\pi(F_i-F_0)t+\Phi_i)}dt,\end{aligned}$$

where the last relation follows from the fact that the integral of the "fast" exponential with frequency F_i+F_0 is approximated by zero. Hence:

$$\begin{aligned}&\left\langle s(t,\Phi_i,h_{\rm CTR}),\frac{1}{\sqrt{T}}e^{+j2\pi F_0 t}\right\rangle\\&=\frac{h_{\rm CTR}}{2\sqrt{T}}e^{+j\Phi_i}\int_T e^{j2\pi(F_i-F_0)t}dt=\frac{\sqrt{T}h_{\rm CTR}}{2}e^{+j\Phi_0}(1-b_i),\end{aligned}\tag{35}$$

where in the last equality, orthogonality is exploited.

Similarly:

$$\begin{aligned}\left\langle s(t,\Phi_i,h_{\rm CTR}),\frac{1}{\sqrt{T}}e^{-j2\pi F_0 t}\right\rangle&=\frac{\sqrt{T}h_{\rm CTR}}{2}e^{-j\Phi_0}(1-b_i),\\\left\langle s(t,\Phi_i,h_{\rm CTR}),\frac{1}{\sqrt{T}}e^{+j2\pi F_1 t}\right\rangle&=\frac{\sqrt{T}h_{\rm CTR}}{2}e^{+j\Phi_1}b_i,\\\left\langle s(t,\Phi_i,h_{\rm CTR}),\frac{1}{\sqrt{T}}e^{-j2\pi F_1 t}\right\rangle&=\frac{\sqrt{T}h_{\rm CTR}}{2}e^{-j\Phi_1}b_i.\end{aligned}\tag{36}$$

The complex exponentials are time-limited in a window of duration T, and thus for $F_i+\frac{20}{T}\ll W$, the orthonormal basis can be safely considered band-limited in the $[-W,W]$ frequency range.

Since $n(t)$ is a circularly symmetric, complex baseband Gaussian random process with PSD $\frac{N_0}{2}$ in the $[-W,W]$ frequency band, its projections on an orthonormal basis (with basis functions limited in the $[-W,W]$ frequency band) will have independent and identically distributed (i.i.d.) circularly symmetric, complex Gaussian components with variance $\frac{N_0}{2}$ [24, pp. 213]:

$$\mathbf{n}=[n_0^+\ n_0^-\ n_1^+\ n_1^-]^T\sim\mathcal{CN}\left(0,\frac{N_0}{2}\mathbf{I}_4\right).\tag{37}$$

■

APPENDIX II

Proof of Theorem 2:

$$\begin{aligned}p(e)&=\int_{\mathbb{R}}\int_{\mathbb{R}}Q\left(\frac{a_{\rm CT}a_{\rm TR}}{\sigma_{\rm CT}\sigma_{\rm TR}}\sqrt{\overline{\rm SNR}}\right)p(a_{\rm TR})p(a_{\rm CT})\ da_{\rm TR}da_{\rm CT}\\&=\int_{\mathbb{R}}\int_{\mathbb{R}}Q\left(\frac{a_{\rm CT}}{\sigma_{\rm CT}}\sqrt{x\ \overline{\rm SNR}}\right)p(x)p(a_{\rm CT})\ dxda_{\rm CT},\end{aligned}\tag{38}$$

where $x\triangleq\frac{a_{\rm TR}^2}{\sigma_{\rm TR}^2}\sim\left|\mathcal{CN}(0,1)\right|^2$, i.e., the square of a unit power Rayleigh random variable, is an exponential random variable with pdf:

$$p(x)=\begin{cases}e^{-x}, & x>0\\0, & \text{otherwise}\end{cases}.\tag{39}$$

Substituting Eq. (39) in Eq. (38):

$$p(e)=\int_{\mathbb{R}}\underbrace{\int_{\mathbb{R}^+}Q\left(\frac{a_{\rm CT}}{\sigma_{\rm CT}}\sqrt{x\ \overline{\rm SNR}}\right)e^{-x}dx}_{=f(a_{\rm CT})}\ p(a_{\rm CT})\ da_{\rm CT}.\tag{40}$$

The inner integral of Eq.(40) can be computed as:

$$f(a_{\rm CT})=\int_{\mathbb{R}^+}Q\left(\sqrt{x\frac{a_{\rm CT}^2}{\sigma_{\rm CT}^2}\ \overline{\rm SNR}}\right)\frac{d}{dx}\left(-e^{-x}\right)dx.$$

Using integration by parts:

$$f(a_{\rm CT})=\frac{1}{2}+\int_{\mathbb{R}^+}e^{-x}\frac{d}{dx}Q\left(\sqrt{x\frac{a_{\rm CT}^2}{\sigma_{\rm CT}^2}\ \overline{\rm SNR}}\right)dx.\tag{41}$$

It can further be shown that [28]:

$$\frac{d}{dx}Q\left(\sqrt{x\frac{a_{\rm CT}^2}{\sigma_{\rm CT}^2}\ \overline{\rm SNR}}\right)=-\sqrt{\frac{\frac{a_{\rm CT}^2}{\sigma_{\rm CT}^2}\ \overline{\rm SNR}}{8\pi}}\frac{1}{\sqrt{x}}e^{-\frac{1}{2}x\frac{a_{\rm CT}^2}{\sigma_{\rm CT}^2}\overline{\rm SNR}}.\tag{42}$$

Combining Eqs. (41)–(42) offers:

$$f(a_{\rm CT})=\frac{1}{2}-\sqrt{\frac{\frac{a_{\rm CT}^2}{\sigma_{\rm CT}^2}\ \overline{\rm SNR}}{8\pi}}\int_{\mathbb{R}^+}\frac{1}{\sqrt{x}}e^{-x\left(\frac{1}{2}\frac{a_{\rm CT}^2}{\sigma_{\rm CT}^2}\overline{\rm SNR}+1\right)}dx,$$

and using the relation $\int_{\mathbb{R}^+}\frac{1}{\sqrt{x}}\exp\{-ax\}\,dx=\sqrt{\frac{\pi}{a}}$ yields

$$f(a_{\rm CT})=\frac{1}{2}-\frac{1}{2}\sqrt{\frac{\frac{a_{\rm CT}^2}{\sigma_{\rm CT}^2}\ \overline{\rm SNR}}{\frac{a_{\rm CT}^2}{\sigma_{\rm CT}^2}\ \overline{\rm SNR}+2}}.\tag{43}$$

Hence, by utilizing Eq. (43) and substituting in Eq. (40), the probability of error is given by:

$$p(e)=\frac{1}{2}-\frac{1}{2}\int_{\mathbb{R}}\sqrt{\frac{\frac{a_{\rm CT}^2}{\sigma_{\rm CT}^2}\ \overline{\rm SNR}}{\frac{a_{\rm CT}^2}{\sigma_{\rm CT}^2}\ \overline{\rm SNR}+2}}\ p(a_{\rm CT})\ da_{\rm CT}.$$

By substituting the pdf of $a_{\rm CT}$:

$$p(e)=\frac{1}{2}-\frac{1}{2}\int_{\mathbb{R}^+}\sqrt{\frac{\frac{a_{\rm CT}^2}{\sigma_{\rm CT}^2}\ \overline{\rm SNR}}{\frac{a_{\rm CT}^2}{\sigma_{\rm CT}^2}\ \overline{\rm SNR}+2}}\ \frac{2a_{\rm CT}}{\sigma_{\rm CT}^2}e^{-\frac{a_{\rm CT}^2}{\sigma_{\rm CT}^2}}\ da_{\rm CT}.\tag{44}$$

Setting $t=\frac{a_{\rm CT}^2}{\sigma_{\rm CT}^2}\ \overline{\rm SNR}/2$, the integral of Eq. (44) can be written as:

$$\begin{aligned}p(e)&=\frac{1}{2}-\frac{1}{2}\int_{\mathbb{R}^+}\sqrt{\frac{t}{t+1}}\frac{2}{\overline{\rm SNR}}e^{-\frac{2}{\overline{\rm SNR}}t}\ dt\\&=\frac{1}{2}-\frac{1}{2}\underbrace{\int_{\mathbb{R}^+}\sqrt{\frac{t}{t+1}}\frac{d}{dt}\left(-e^{-\frac{2}{\overline{\rm SNR}}t}\right)\ dt}_{=A}.\end{aligned}\tag{45}$$

Using integration by parts, the integral of Eq. (45) can be simplified to:

$$A = \int_{\mathbb{R}^+} \frac{1}{2} t^{-\frac{1}{2}} (t+1)^{-\frac{3}{2}} e^{-\frac{2}{\overline{\mathrm{SNR}}} t} \, dt. \tag{46}$$

Substituting the above back in Eq. (45):

$$\begin{aligned} p(e) &= \frac{1}{2} - \frac{1}{2} \int_{\mathbb{R}^+} \frac{1}{2} t^{-\frac{1}{2}} (t+1)^{-\frac{3}{2}} e^{-\frac{2}{\overline{\mathrm{SNR}}} t} \, dt \\ &= \frac{1}{2} - \frac{\sqrt{\pi}}{4} \mathrm{U}\left(\frac{1}{2}, 0, \frac{2}{\overline{\mathrm{SNR}}}\right), \end{aligned} \tag{47}$$

where $\mathrm{U}(a,b,z)$ denotes the *confluent hypergeometric* U function, given in integral form as:

$$\mathrm{U}(a,b,z) = \frac{1}{\Gamma(a)} \int_{\mathbb{R}^+} e^{-zt} t^{a-1} (t+1)^{b-a-1} \, dt. \tag{48}$$

■

APPENDIX III

Proof of Theorem 3:

It is assumed that coherence time, T_{coh}, is known; hence, to achieve a fully interleaved system the value of depth D is set

$$(D + N_{\mathrm{tr}})T = T_{\mathrm{coh}}. \tag{49}$$

The transmitter stores D codewords belonging to a linear block code $\mathcal{C}$ in a $D \times n$ matrix and transmits the information column-wise. For each D bits (each column of interleaving matrix), N_{tr} training bits are utilized for channel estimation. Thus, the transmitter sends at total $n(D + N_{\mathrm{tr}})$ bits.

The receiver has $n(D + N_{\mathrm{tr}})$ received symbols; nN_{tr} of them correspond to training bits to estimate the random channel vectors associated with each column of interleaving matrix. Let $\mathbf{h}_1, \mathbf{h}_2, \ldots, \mathbf{h}_n$ be the actual compound channel vectors associated with the symbols of the 1st, 2nd, ..., n-th column of interleaving matrix, respectively. Due to Eq. (49) the compound channel vectors are independent of each other (and identically distributed).

We conclude that in fully interleaved system the receiver decodes symbol sequences that correspond to codewords with coded bits experiencing independent fading. Accordingly with Eq. (30), the received signal for a single row of interleaving matrix can be expressed as

$$\mathbf{r}_i = \mathbf{h}_i \odot \mathbf{s}_{c_i} + \mathbf{n}_i, \quad i = 1, 2, \ldots, n, \tag{50}$$

with $\mathbf{c} = [c_1 \; c_2 \; \ldots \; c_n] \in \mathcal{C}$ denoting the transmitted codeword associated with the specific row of interleaving matrix and $\mathbf{s}_{c_i} = \begin{bmatrix} 1-c_i & 1-c_i & c_i & c_i \end{bmatrix}^T$, $i = 1, \ldots, n$.

Assuming perfect knowledge of $\mathbf{h}_1, \ldots, \mathbf{h}_n$, and exploiting their independence, the average probability of decoding error is given by

$$\begin{aligned} p(e) &= \int_{\mathbf{h}_1} \cdots \int_{\mathbf{h}_n} p(e|\mathbf{h}_1, \ldots, \mathbf{h}_n) p(\mathbf{h}_1) \ldots p(\mathbf{h}_n) d\mathbf{h}_1 \ldots d\mathbf{h}_n \\ &= \mathop{\mathbb{E}}_{\mathbf{h}_1, \ldots, \mathbf{h}_n} \left\{ p(e|\mathbf{h}_1, \ldots, \mathbf{h}_n) \right\}. \end{aligned} \tag{51}$$

Let $\mathbf{h}_{1:n} = [\mathbf{h}_1^T \; \mathbf{h}_2^T \; \ldots \; \mathbf{h}_n^T]^T$ for simplicity. For each $i = 1, \ldots, n$, the log-likelihood ratio associated with vector $\mathbf{r}_i$ (which is a proper complex Gaussian given $c_i, \mathbf{h}_i$) can be written as

$$l_i = \ln\left(\frac{p(\mathbf{r}_i|c_i=0,\mathbf{h}_i)}{p(\mathbf{r}_i|c_i=1,\mathbf{h}_i)}\right) = \frac{4}{N_0} \Re\left\{ \left(\mathbf{h}_i \odot \left(\mathbf{s}_0 - \mathbf{s}_1\right)\right)^H \mathbf{r}_i \right\}. \tag{52}$$

After some algebra and using Eqs. (8) and (14), the conditional p.d.f. of l_i can be expressed as

$$p(l_i|c_i=0,\mathbf{h}_i) \equiv \mathcal{N}\left(2\overline{\mathrm{SNR}} \frac{a_{\mathrm{CT},i}^2 a_{\mathrm{TR},i}^2}{\sigma_{\mathrm{CT}}^2 \sigma_{\mathrm{TR}}^2}, 4\overline{\mathrm{SNR}} \frac{a_{\mathrm{CT},i}^2 a_{\mathrm{TR},i}^2}{\sigma_{\mathrm{CT}}^2 \sigma_{\mathrm{TR}}^2} \right), \tag{53}$$

$$p(l_i|c_i=1,\mathbf{h}_i) \equiv \mathcal{N}\left(-2\overline{\mathrm{SNR}} \frac{a_{\mathrm{CT},i}^2 a_{\mathrm{TR},i}^2}{\sigma_{\mathrm{CT}}^2 \sigma_{\mathrm{TR}}^2}, 4\overline{\mathrm{SNR}} \frac{a_{\mathrm{CT},i}^2 a_{\mathrm{TR},i}^2}{\sigma_{\mathrm{CT}}^2 \sigma_{\mathrm{TR}}^2} \right), \tag{54}$$

where the parameters $a_{\mathrm{CT},i}, a_{\mathrm{TR},i}$ are associated with compound channel $\mathbf{h}_i$, $i = 1, 2, \ldots, n$. Thus, for the channel described by (50), the following is satisfied:

$$p(l_i|c_i=0,\mathbf{h}_i) = p(-l_i|c_i=1,\mathbf{h}_i), \quad i = 1, 2, \ldots, n, \tag{55}$$

and the channel is memoryless given $\mathbf{h}_{1:n}$; thus, it can be considered as a binary-input symmetric-output channel [29].

Under equiprobable signaling, due to the linearity of block code $\mathcal{C}$ and the memoryless structure of channel given $\mathbf{h}_{1:n}$, the conditional probability of decoding error is upper bounded by [30, Eqs. (2)–(4)]

$$p(e|\mathbf{h}_{1:n}) \leq \sum_{d=d_{\min}}^{n} N_d(\mathcal{C}) \, \Pr\left(\left(\sum_{i=1}^{d} l_i \right) < 0 \middle| \mathbf{c} = \mathbf{0}, \mathbf{h}_{1:n} \right), \tag{56}$$

where $N_d(\mathcal{C})$ is the number of codewords in $\mathcal{C}$ that have Hamming weight d, i.e.,

$$N_d(\mathcal{C}) = \left| \left\{ \mathbf{c} \in \mathcal{C} : w_{\mathrm{H}}(\mathbf{c}) = d \right\} \right|. \tag{57}$$

The symmetry of channel (Eq. (55)) ensures that no loss of optimality is incurred by considering the all-zero codeword in the pairwise error probability at the right-hand side of (56).

Under the assumption of all-zero codeword and for given $\mathbf{h}_{1:n}$ the p.d.f. of random variable (RV) $l = \sum_{i=1}^{d} l_i$ is

$$p(l|\mathbf{c}=\mathbf{0},\mathbf{h}_{1:n}) \equiv \mathcal{N}\left(2\overline{\mathrm{SNR}} \sum_{i=1}^{d} w_i^2 v_i^2, 4\overline{\mathrm{SNR}} \sum_{i=1}^{d} w_i^2 v_i^2 \right), \tag{58}$$

where RVs $w_i = \frac{a_{\mathrm{CT},i}}{\sigma_{\mathrm{CT}}}$ and $v_i = \frac{a_{\mathrm{TR},i}}{\sigma_{\mathrm{TR}}}$ are independent and follow Rayleigh distribution with unit power.

In view of Eqs. (56) and (58) the conditional probability of decoding error satisfies

$$\begin{aligned} p(e|\mathbf{h}_{1:n}) &\leq \sum_{d=d_{\min}}^{n} N_d(\mathcal{C}) \; Q\left(\sqrt{ \overline{\mathrm{SNR}} \sum_{i=1}^{d} w_i^2 v_i^2 } \right) \\ &\leq \frac{1}{2} \sum_{d=d_{\min}}^{n} N_d(\mathcal{C}) \; \exp\left(-\frac{1}{2} \overline{\mathrm{SNR}} \sum_{i=1}^{d} w_i^2 v_i^2 \right). \end{aligned} \tag{59}$$

Eq. (59) stems from the identity $X \sim \mathcal{N}(\mu, \sigma^2) \implies \Pr(X < 0) = Q\left(\frac{\mu}{\sigma}\right)$ and from the Chernoff bound for the Q function, $Q(x) \leq \frac{1}{2} e^{-\frac{1}{2}x^2}$. It is noted that the upper bound depends

solely on the random amplitudes $a_{\mathrm{CT},i}, a_{\mathrm{TR},i}, \forall i$, which must be eliminated through expectation to obtain the upper bound on the probability of decoding error. In view of Eqs. (59) and (51), $p(e)$ is upper bounded by

$$p(e) \leq \mathop{\mathbb{E}}_{\mathbf{h}_{1:n}} \left\{ \frac{1}{2} \sum_{d=d_{\min}}^{n} N_d(\mathcal{C}) \ \exp\left(-\frac{1}{2}\overline{\mathrm{SNR}} \sum_{i=1}^{d} w_i^2 v_i^2 \right) \right\}$$
$$= \frac{1}{2} \sum_{d=d_{\min}}^{n} N_d(\mathcal{C}) \mathop{\mathbb{E}}_{\mathbf{h}_{1:n}} \left\{ \exp\left(-\frac{1}{2}\overline{\mathrm{SNR}} \sum_{i=1}^{d} w_i^2 v_i^2 \right) \right\}$$
$$= \frac{1}{2} \sum_{d=d_{\min}}^{n} N_d(\mathcal{C}) \prod_{i=1}^{d} \mathop{\mathbb{E}}_{w_i,v_i} \left\{ \exp\left(-\frac{\overline{\mathrm{SNR}}}{2} w_i^2 v_i^2 \right) \right\}. \quad (60)$$

The quantity $\mathop{\mathbb{E}}_{w_i,v_i} \left\{ \exp\left(-\frac{\overline{\mathrm{SNR}}}{2} w_i^2 v_i^2 \right) \right\}$ is calculated as

$$\mathop{\mathbb{E}}_{w_i,v_i} \left\{ \exp\left(-\frac{1}{2}\overline{\mathrm{SNR}} w_i^2 v_i^2 \right) \right\}$$
$$= \int_0^\infty \int_0^\infty \exp\left(-\frac{1}{2}\overline{\mathrm{SNR}} w_i^2 v_i^2 \right) 4 w_i v_i \exp(-w_i^2 - v_i^2) dw_i dv_i$$
$$= \int_0^\infty 4 \frac{v_i \exp(-v_i^2)}{2 + v_i^2 \overline{\mathrm{SNR}}} dv_i = \int_0^\infty 2 \frac{\exp(-v_i)}{2 + v_i \overline{\mathrm{SNR}}} dv_i \quad (61)$$
$$= \left(\frac{2}{\overline{\mathrm{SNR}}} \right) \exp\left(\frac{2}{\overline{\mathrm{SNR}}} \right) \Gamma\left(0, \frac{2}{\overline{\mathrm{SNR}}} \right). \quad (62)$$

Eqs. (3.461.3) and (3.383.10) in [31] are utilized to obtain Eqs. (61) and (62), respectively. $\Gamma(s,x) = \int_x^\infty t^{s-1} e^t dt$ is the upper incomplete gamma function. Substituting (62) in (60), the final upper bound of $p(e)$ is expressed as

$$p(e) \leq \frac{1}{2} \sum_{d=d_{\min}}^{n} N_d(\mathcal{C}) \left(\frac{2 \exp\left(\frac{2}{\overline{\mathrm{SNR}}} \right) \Gamma\left(0, \frac{2}{\overline{\mathrm{SNR}}} \right)}{\overline{\mathrm{SNR}}} \right)^d. \quad (63)$$

To prove the diversity order argument, the definition of diversity order in [32, Eq. 3] will be utilized. Specifically, the quantity

$$\lim_{\overline{\mathrm{SNR}} \to \infty} \frac{\log\left(\frac{2 \exp\left(\frac{2}{\overline{\mathrm{SNR}}} \right) \Gamma\left(0, \frac{2}{\overline{\mathrm{SNR}}} \right)}{\overline{\mathrm{SNR}}} \right)}{\log(\overline{\mathrm{SNR}})}$$
$$= \lim_{\overline{\mathrm{SNR}} \to \infty} \left\{ \frac{\log\left(\frac{2}{\overline{\mathrm{SNR}}} \right)}{\log(\overline{\mathrm{SNR}})} + \frac{\log\left(\exp\left(\frac{2}{\overline{\mathrm{SNR}}} \right) \right)}{\log(\overline{\mathrm{SNR}})} + \frac{\log\left(\Gamma\left(0, \frac{2}{\overline{\mathrm{SNR}}} \right) \right)}{\log(\overline{\mathrm{SNR}})} \right\} \quad (64)$$

equals -1, because the first term of the right-hand side of (64) offers -1, the second offers 0, and the third offers 0 if we use L'Hôpital's rule and Eq. (8.8.13) in [33, pp. 178]. Therefore,

$$\lim_{\overline{\mathrm{SNR}} \to \infty} \frac{\log\left(\frac{2 \exp\left(\frac{2}{\overline{\mathrm{SNR}}} \right) \Gamma\left(0, \frac{2}{\overline{\mathrm{SNR}}} \right)}{\overline{\mathrm{SNR}}} \right)^d}{\log(\overline{\mathrm{SNR}})} = -d \quad (65)$$

Using (8.4.4) and (6.8.2) in [33] we conclude that $\left(\frac{2 \exp\left(\frac{2}{\overline{\mathrm{SNR}}} \right) \Gamma\left(0, \frac{2}{\overline{\mathrm{SNR}}} \right)}{\overline{\mathrm{SNR}}} \right) \leq 1$ for every (non-negative) value of $\overline{\mathrm{SNR}}$. Hence, the function

$$\left(\frac{2 \exp\left(\frac{2}{\overline{\mathrm{SNR}}} \right) \Gamma\left(0, \frac{2}{\overline{\mathrm{SNR}}} \right)}{\overline{\mathrm{SNR}}} \right)^d \quad (66)$$

is a non-increasing function of d. Thus, combining Eqs. (63) and (65) completes the proof. ■

REFERENCES

[1] I. Akyildiz, W. Su, Y. Sankarasubramaniam, and E. Cayirci, "Wireless sensor networks: A survey," *Computer Networks*, vol. 38, no. 4, pp. 393–422, Mar. 2002.

[2] H. Stockman, "Communication by means of reflected power," *Proc. IRE*, pp. 1196–1204, 1948.

[3] G. Vannucci, A. Bletsas, and D. Leigh, "A software-defined radio system for backscatter sensor networks," *IEEE Trans. Wireless Commun.*, vol. 7, no. 6, pp. 2170–2179, Jun. 2008.

[4] D. Yeager, A. Sample, J. Smith, P. Powledge, and A. Mamishev, "Sensor applications in RFID technology," in *Proc. International Conference on Actual Problems of Electron Devices Engineering (APEDE)*, Saratov, Russia, Sep. 2006, pp. 449–452.

[5] S. Kim, M. M. Tentzeris, A. Traille, H. Aubert, and A. Georgiadis, "A dual-band retrodirective reflector array on paper utilizing substrate integrated waveguide (SIW) and inkjet printing technologies for chipless RFID tag and sensor applications," in *Proc. IEEE Int. Symp. on Antennas and Propagation*, Orlando, FL, Jul. 2013, pp. 2301–2302.

[6] J. D. Griffin and G. D. Durgin, "Complete link budgets for backscatter-radio and RFID systems," *IEEE Trans. Antennas Propagat.*, vol. 51, no. 2, pp. 11–25, Apr. 2009.

[7] J. Kimionis, A. Bletsas, and J. N. Sahalos, "Increased range bistatic scatter radio," *IEEE Trans. Commun.*, vol. 62, no. 3, pp. 1091–1104, Mar. 2014.

[8] C. Angerer, R. Langwieser, and M. Rupp, "RFID reader receivers for physical layer collision recovery," *IEEE Trans. Commun.*, vol. 58, no. 12, pp. 3526–3537, Dec. 2010.

[9] A. Bletsas, J. Kimionis, A. G. Dimitriou, and G. N. Karystinos, "Single-antenna coherent detection of collided FM0 RFID signals," *IEEE Trans. Commun.*, vol. 60, no. 3, pp. 756–766, 2012.

[10] A. Sample, D. Yeager, J. Smith, P. Powledge, and A. Mamishev, "Energy harvesting in RFID systems," in *Proc. International Conference on Actual Problems of Electron Devices Engineering (APEDE)*, Saratov, Russia, Sep. 2006, pp. 445–449.

[11] A. Sample, J. Braun, A. Parks, and J. Smith, "Photovoltaic enhanced UHF RFID tag antennas for dual purpose energy harvesting," in *Proc. IEEE Int. Conf. on RFID*, Orlando, FL, Apr. 2011, pp. 146–153.

[12] A. Boaventura, A. Collado, A. Georgiadis, and N. B. Carvalho, "Spatial power combining of multi-sine signals for wireless power transmission applications," *IEEE Trans. Microwave Theory Tech.*, vol. 62, no. 4, pp. 1022–1030, Apr. 2014.

[13] J. Kimionis, A. Bletsas, and J. N. Sahalos, "Design and implementation of RFID systems with software defined radio," in *in Proc. IEEE European Conf. on Antennas and Propagation (EuCAP)*, Prague, Czech Republic, Mar. 2012, pp. 3464–3468.

[14] ——, "Bistatic backscatter radio for power-limited sensor networks," in *Proc. IEEE Global Commun. Conf. (Globecom)*, Atlanta, GA, Dec. 2013, pp. 353–358.

[15] V. Liu, A. Parks, V. Talla, S. Gollakota, D. Wetherall, and J. R. Smith, "Ambient backscatter: Wireless communication out of thin air," in *ACM SIGCOMM 2013*, Hong Kong, China, 2013, pp. 39–50.

[16] E. Kampianakis, J. Kimionis, K. Tountas, C. Konstantopoulos, E. Koutroulis, and A. Bletsas, "Wireless environmental sensor networking with analog scatter radio & timer principles," *IEEE Sensors J.*, vol. 14, no. 10, pp. 3365–3376, Oct. 2014.

[17] P. N. Alevizos, N. Fasarakis-Hilliard, K. Tountas, N. Agadakos, N. Kargas, and A. Bletsas, "Channel coding for increased range bistatic backscatter radio: Experimental results," in *Proc. IEEE RFID Technology and Applications (RFID-TA)*, Tampere, Finland, Sep. 2014, pp. 38–43.

[18] S. Thomas, E. Wheeler, J. Teizer, and M. Reynolds, "Quadrature amplitude modulated backscatter in passive and semipassive UHF RFID systems," *IEEE Trans. Microwave Theory Tech.*, vol. 60, no. 4, pp. 1175–1182, Apr. 2012.

[19] A. Bletsas, A. G. Dimitriou, and J. N. Sahalos, "Improving backscatter radio tag efficiency," *IEEE Trans. Microwave Theory Tech.*, vol. 58, no. 6, pp. 1502–1509, Jun. 2010.

[20] J. Kimionis, "Bistatic scatter radio for increased-range environmental sensing," Master's thesis, Technical University of Crete, Aug. 2013, supervisor A. Bletsas.

[21] E. Kampianakis, "Scatter radio sensor network with analog frequency modulation principles," Master's thesis, Technical University of Crete, Jul. 2014, supervisor A. Bletsas.
[22] S. M. Kay, *Fundamentals of statistical signal processing. [Volume I]. , Estimation theory*. Upper Saddle River (N.J.): Prentice Hall, 1993.
[23] J. D. Griffin and G. D. Durgin, "Gains for RF tags using multiple antennas," *IEEE Trans. Antennas Propagat.*, vol. 56, no. 2, pp. 563–570, Feb. 2008.
[24] J. G. Proakis and M. Salehi, *Digital Communications*, 5th ed. New York, NY: McGraw-Hill, 2007.
[25] P. N. Alevizos and A. Bletsas, "Noncoherent composite hypothesis testing receivers for extended range bistatic scatter radio WSNs," in *Proc. IEEE Int. Conf. on Commun. (ICC)*, London, UK, Jun. 2015.
[26] P. Stoica and R. L. Moses, *Introduction to spectral analysis*. Upper Saddle River, N.J.: Prentice Hall, 1997.
[27] R. J. McEliece, *The Theory of Information and Coding*, 2nd ed. New York, NY: Cambridge University Press, 2001.
[28] N. Fasarakis-Hilliard, "Coherent detection and channel coding for backscatter sensor networks," Master's thesis, Technical University of Crete, Aug. 2014, supervisor A. Bletsas.
[29] T. Richardson and R. Urbanke, *Modern Coding Theory*. Cambridge University Press, 2008.
[30] A. Martinez, A. G. i Fabregas, and G. Caire, "Error probability analysis of bit-interleaved coded modulation." *IEEE Trans. Inform. Theory*, vol. 52, no. 1, pp. 262–271, Jan. 2006.
[31] I. S. Gradshteyn and I. M. Ryzhik, *Table of integrals, series, and products*, 7th ed. Elsevier/Academic Press, Amsterdam, 2007.
[32] L. Zheng and D. N. C. Tse, "Diversity and multiplexing: A fundamental tradeoff in multiple antenna channels," *IEEE Trans. Inform. Theory*, vol. 49, no. 5, pp. 1073–1096, May 2003.
[33] F. W. J. Olver, D. W. Lozier, R. F. Boisvert, and C. W. Clark, *NIST handbook of mathematical functions*. New York, NY: Cambridge Univ. Press, 2010.

Nikos Fasarakis-Hilliard received his diploma degree and MSc in Electronic and Computer Engineering from the Technical University of Crete, Greece, in 2012 and 2014, respectively. He is currently a PhD candidate at the Computing Science Department, University of Alberta.

His research interests lie at the confluence of wireless sensor networking, signal processing, convex optimization and low complexity algorithmic designs.

Panos N. Alevizos (S'14) was born in Athens, Greece, in 1988. He received his Engineering Diploma and M.Sc. in Electronic and Computer Engineering from Technical University of Crete (TUC), Greece, in 2012 and 2014, respectively. He is is currently pursuing a PhD degree at TUC and he is working as a graduate researcher with the Telecom Lab.

His research interests include communication theory with emphasis on backscatter radio and RFID, the area of wireless communications and networking, estimation and detection theory, information and coding theory, and probabilistic inference. He has developed low-complexity detection and decoding algorithms using software-defined radios for backscatter radio communications.

Aggelos Bletsas (S'03-M'05-SM'14) received with excellence his diploma degree in Electrical and Computer Engineering from Aristotle University of Thessaloniki, Greece in 1998, and the S.M. and Ph.D. degrees from Massachusetts Institute of Technology in 2001 and 2005, respectively. He worked at Mitsubishi Electric Research Laboratories (MERL), Cambridge MA, as a Postdoctoral Fellow and at Radiocommunications Laboratory (RCL), Department of Physics, Aristotle University of Thessaloniki, as a Visiting Scientist. He joined School of Electronic and Computer Engineering, Technical University of Crete, in summer of 2009, as an Assistant Professor, and promoted to Associate Professor at the beginning of 2014.

His research interests span the broad area of scalable wireless communication and networking, with emphasis on relay techniques, backscatter communications and RFID, energy harvesting, radio hardware/software implementations for wireless transceivers and low-cost sensor networks. His current vision and focus is on single-transistor front-ends and backscatter sensor networks, for LARGE-scale environmental sensing. He is the principal investigator (PI) of project BLASE: Backscatter Sensor Networks for Large-Scale Environmental Sensing, funded from the General Secretariat of Research & Technology Action Proposals evaluated positively from the 3rd European Research Council (ERC) Call. He is also Management Committee (MC) member and National Representative in the European Union COST Action IC1301 Wireless Power Transmission for Sustainable Electronics (WiPE). He is Associate Editor of IEEE Wireless Communication Letters since its foundation and Technical Program Committee (TPC) member of flagship IEEE conferences. He holds two patents from USPTO and he was recently included in https://sites.google.com/site/highlycited/highly-cited-greek-scientists.

Dr. Bletsas was the co-recipient of IEEE Communications Society 2008 Marconi Prize Paper Award in Wireless Communications, best paper distinction in ISWCS 2009, Siena, Italy, Second Best Student Paper Award in the IEEE RFID-TA 2011, Sitges, Barcelona, Spain and best paper distinction in IEEE Sensors Conference (SENSORS), November 2013, Baltimore, USA. Two of his undergraduate advisees were winners of the 2009-2011 and 2011-2012 best Diploma Thesis contest, respectively, among all Greek Universities on "Advanced Wireless Systems", awarded by IEEE VTS/AES joint Greek Chapter. At the end of 2013, Dr. Bletsas was awarded the Technical University of Crete 2013 Research Excellence Award.